Demonstration of a spaced-antenna weather radar using an X-band active phased-array

V. Venkatesh†, K. Orzel †, S. Frasier†
† University of Massachusetts, Amherst, MA.

Abstract—
Spaced-antenna retrievals are a potential means of higher spatial-resolution wind-field retrievals than currently available single weather radar techniques. Relevant literature to date has focused on theoretical, numerical [1][2] or engineering aspects [3]. Herein, we present an empirical case study of weather radar spaced-antenna retrievals using an X-band active phased array. On a stratiform rain dataset, spaced-antenna (SA) measurements are compared to Doppler beam swinging (DBS) and Velocity Azimuth Display (VAD)-like retrievals of baseline wind. Using Monte-Carlo simulations to determine data quality thresholds, spaced-antenna retrievals (G-SZL and FSA algorithms) are compared to DBS and VAD-like retrievals of baseline wind. The time-domain Slope at Zero-Lag (G-SZL) algorithm had a lower rms error (0.56 m/s) than the Full Spectral Analysis (FSA) algorithm (0.83 m/s). This is because the G-SZL algorithm is parametric and has good immunity to errors in the discrete correlation coefficient estimates. The correlation between the G-SZL and DBS retrievals was 0.85. The correlation between G-SZL and VAD retrievals was 0.83. These results demonstrate reasonable fidelity for spaced-antenna weather radar retrievals at low to moderate wind-speeds and relatively close range (i.e. upto 10 Km). For larger wind-speeds and spatially varying wind-profiles at farther ranges, none of the single radar wind-field retrieval methods considered herein perform adequately.

Index Terms—**weather radar, phased array, spaced antenna.**

I. Introduction

Since the first use of Doppler weather radars, research on radar algorithms and technology have continually improved their performance [4]. The advent of phased-array weather radars have enabled several new capabilities. Some examples follow. The ability of phased-array radars to multiplex between locations has improved data quality, when the echo coherence time is comparable to the dwell time [5]. Kalman filtering techniques to assimilate data over short rapid-scan time-scales [6] have been shown to improve storm forecasting skill. Recently, adaptive signal processing techniques for instantaneous imaging of precipitation events have also been demonstrated [7]. This work is a case study demonstration of a high spatial-resolution wind-field retrieval technique using phased-array radar technology.

The employed technique is the so-called spaced-antenna (SA) method which retrieves the wind-field by correlating the electric fields at two displaced apertures [8][9]. The ability to segment the active array face into multiple displaced antennas allows for implementation of this technique. In principle, the SA method is capable of higher spatial-resolution retrievals than single radar methods currently in use in the weather radar community. This is because existing wind-field retrievals methods rely on the scanning capability of weather radars to retrieve the large spatial-scale wind-field (e.g. VAD [10] and TREC methods [11]).

The SA method was originally developed to profile plasma inhomogeneities in the Ionosphere and has since been successfully employed for clear-air observations of the convective boundary layer. Interest in applying this method to profile precipitation is relatively recent. To date, literature on spaced-antenna weather radars has either been theoretical [2][12] or based on numerical simulations [1]. Although there have been studies on engineering aspects of spaced-antenna aperture synthesis [3], empirical studies evaluating the precision of SA retrievals on precipitation echoes have not been reported in the formal literature.

Herein, we evaluate the precision of spaced-antenna retrievals on precipitation echoes using data collected with an X-band phased-array weather radar. Velocity Azimuth Display (VAD) and Doppler beam swinging (DBS) retrievals are used as prognostics. In the following section, we describe the experimental setup and data processing methodology. We then present a comparative analysis of time-domain and spectral spaced-antenna retrieval algorithms.

II. Methodology

A. Experiment description

The University of Massachusetts has developed an active phased-array radar system capable applying weights to each array element on transmit and receive [3]. For spaced antenna aperture synthesis, alternating receive signals from the left and right sub-arrays are interleaved on a pulse-by-pulse basis [1] (system parameters are in table 1). Fig. 1a illustrates the executed experiment to compare spaced-antenna retrievals to Doppler beam swinging and VAD-like retrievals of baseline wind. The antenna motion is in discrete steps of 5 degrees, such that there is no mechanical slew during the duration of the dwell. During each dwell of 1.8s, interleaved I/Q data from the left and right-sub arrays are logged. Using this data, spaced-antenna retrievals of baseline wind are compared to coarser azimuthal-resolution baseline-wind retrievals. Fig. 1b

This work was supported by the National Science Foundation under grants AGS-0937768 and AGS-1318148 to the University of Massachusetts. At the time of publication, the corresponding author is with the Jet Propulsion Laboratory, California Institute of Technology, CA. Corresponding author Email : vijay.venkatesh@jpl.nasa.gov .

TABLE I: X-band phased array spaced antenna system.

Pulse repetition frequency	5 kHz
Effective spaced antenna baseline	8 cm
Equivalent azimuthal 3-dB beamwidth	2.7 degrees
Dwell time	1.8 seconds
Radar frequency	9.36 GHz

illustrates the data processing methodology employed herein. Monte-Carlo based simulations are used to validate the algorithm implementations and synthesize data quality thresholds for analysis. This simulated data path is indicated by "dashed-lines" and the real data path by "solid-lines" in Fig. 1. For every beam location, complex I/Q data is read and stored in a 2-D array. The two dimensions of this array correspond to "fast-time" (range) and "slow-time" (pulse number). The I/Q data is first compressed in fast time using standard matched filtering and windowing methods. Following this the data is "de-interleaved" to separate pulses corresponding to left and right apertures. Auto- and cross-spectra (or equivalently, correlation functions) are then estimated to yield Doppler velocity and SA retrievals. Addtionally, Doppler Beam Swinging (DBS) and Velocity-Azimuth Display (VAD) retrievals of baseline wind are used as prognostics to evaluate the fidelity of spaced-antenna retrievals.

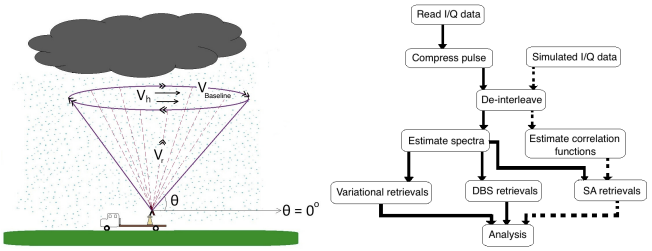

Fig. 1: Top (a) - Illustration of experiment to compare spaced-antenna retrievals with Doppler Beam swinging and VAD-like variational retrievals. A "stepped" mechanical scan is performed at an elevation α = 10 degrees. Azimuthal sampling was every 5 degrees and there was no mechanical slewing during the dwell. Bottom (b) - Illustration of methodology employed to analyze precision of weather radar spaced-antenna retrievals. Algorithm implementations are tested with simulations and determine data quality thresholds for analysis.

B. Data processing algorithms

The Slope at Zero-Lag spaced-antenna algorithm estimates the baseline wind $\widehat{v}_x$ by assuming a Gaussian function form for the correlation functions (G-SZL), where the retrieval is accessed by [1]

$$\widehat{v}_{xG-SZL} = \frac{1}{2k^2\sigma_{e\phi}^2}\frac{\widehat{\tau}_p}{\widehat{\tau}_c^2}. \tag{1}$$

Here, $\widehat{\tau}_p$ and $\widehat{\tau}_c$ represent estimates of time-lag to cross-correlation peak and auto-correlation width respectively. Note that τ_p/τ_c^2 is mathematically equivalent to the normalized slope at zero-lag for Gaussian correlation functions [13]. Invoking this equivalence is necessary at X-band because direct finite difference estimators of slope at zero-lag are impractical due to insufficient sampling of the correlation function. By contrast, the Full Spectral analysis (FSA) spaced-antenna algorithm retrieves the baseline wind using the relationship [9]

$$\widehat{v}_{xFSA} = \frac{1}{2k^2\sigma_{e\phi}^2\frac{\Delta x}{2k}}\widehat{m}\widehat{\sigma}_w^2. \tag{2}$$

Here, $\widehat{m}$ is the slope of the cross spectral phase in the Doppler velocity domain and $\widehat{\sigma}_w$ is the Doppler spectrum width. We note that although the FSA algorithm operates in complementary domain to the G-SZL algorithm and uses different estimators, it has been shown to be a non-parametric implementation of the slope at zero-lag family [1].

The Doppler Beam Swinging (DBS) method retrieves the wind-field directly from two radial velocity observations (denote by $\widehat{v}_{r1}$ and $\widehat{v}_{r2}$ respectively) separated by some scan angle ϕ_{DBS}. The cross-beam wind is retrieved as

$$\widehat{v}_{DBS} = \widehat{v}_{r1}\tan\phi_{DBS} + \frac{\widehat{v}_{r2} - \frac{\widehat{v}_{r1}}{\cos\phi_{DBS}}}{\sin\phi_{DBS}} \tag{3}$$

where, $\widehat{v}_{DBS}$ denotes the DBS retrieval. For small beam swing angles, (1) can be approximated as [14]

$$\widehat{v}_{DBS} = \frac{\widehat{v}_{r_2} - \widehat{v}_{r_1}}{\phi_{DBS}} \tag{4}$$

Based on [2], spaced-antenna measurements of mean baseline wind are limited by radial velocity shear within the resolution volume. However, DBS retrievals are also affected by the same error source. To show this, consider a wind-field characterized by mean radial and baseline components v_z and v_x respectively. Denote the uniform shear of the $z-$component of velocity along x as s_{zx} and shear of the $x-$component of velocity along x as s_{xx}. We define a coordinate system such that for some scan angle ψ, v_z is the radial velocity and v_x is the baseline velocity. Now, the measured radial velocities at the two scan angles ψ and $\psi + \phi_{DBS}$ are given by,

$$\langle\widehat{v}_{r1}\rangle = v_z \tag{5}$$

$$\langle\widehat{v}_{r2}\rangle = (v_z + r_0 s_{zx}\tan\phi_{DBS})\cos\phi_{DBS} + (v_x + r_0 s_{xx})\sin\phi_{DBS} \tag{6}$$

where, r_0 is range to the resolution volume, $\widehat{V}_{r_1}$ and $\widehat{V}_{r_2}$ are radial velocities estimates from two look angles ψ_1 and ψ_2 separated by some scan angle ϕ_{DBS}. For small scan angles, $tan\phi_{DBS} \approx sin\phi_{DBS} \approx \phi_{DBS}$ and $\cos\phi_{DBS} \approx 1$. The expression for v_{r2} therefore simplifies to

$$\langle\widehat{v}_{r2}\rangle = v_z + [v_x + r_0(s_{zx} + s_{xx})]\phi_{DBS} \tag{7}$$

' Substituting (5) and (7) in (4), the expectation of the Doppler beam swinging retrieval reduces to

$$\langle\widehat{v}_{DBS}\rangle = v_x + r_0(s_{xx} + s_{zx}) \tag{8}$$

where, $\widehat{v}_{DBS}$ denotes the Doppler beam swinging retrieval. In arriving at equation (8), we have assumed that the scale of the swing (i.e. $r_0\phi_{DBS}$) is smaller than the scale of variation

of s_x. Further, we note that the expectation of the SA retrievals in the presence of velocity shear can be approximated by $v_x + r_0 s_{zx}$ [2]. The net result of all this is that the DBS retrievals serve as a prognostic to benchmark SA baseline wind retrievals, provided the shear of the x-component of velocity along the plane of the scan is negligible (i.e. $s_{xx} \approx 0$).

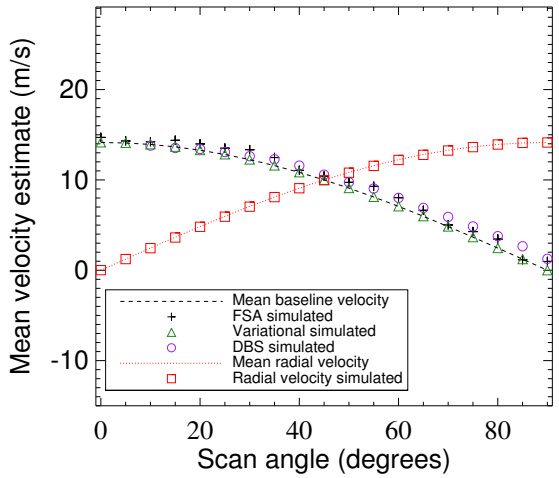

Fig. 2: Mean simulated retrievals from various algorithms employed in this work. Instrumental parameters are as in Table 1. v_z and v_x projections are indicated by the "dotted" and "dashed" lines respectively. Results are from 100 Monte-Carlo trials with an RMS velocity turbulence of 2 m/s, SNR of 4 dB and v_y = 10 m/s. Note that the v_z and v_x components are in quadrature for a spatially invariant wind-field.

To address sector scans, the VAD implementation in this work retrieves the mean wind-field from a least squares fit to radial velocity observations [10]. For N looks over the azimuth span, let the radial velocity estimates of the precipitation echoes be represented as $\widehat{v}_{r_n}$ and fits to the radial velocity observations be $v_{r_{fit}}$. Let the corresponding azimuthal angles be represented by ϕ_n, where $n = 1, 2, 3, ..., N$.

$$v_{r_{fit}} = \widehat{a}_0 + \widehat{a}_1 \cos(\widehat{\Omega}_1 + \phi_n) + a_2 \cos(\widehat{\Omega}_2 + 2\phi_n) \quad (9)$$

In matrix form, this becomes

$$\left[v_{r_{fit}}\right] = \left[\begin{array}{ccc} 1 & \cos(\widehat{\Omega}_1 + \phi) & \cos(\widehat{\Omega}_2 + \phi) \end{array}\right] \left[\begin{array}{c} \widehat{a}_0 \\ \widehat{a}_1 \\ \widehat{a}_2 \end{array}\right] \quad (10)$$

Here $\widehat{a}_0$, $\widehat{a}_1$ and $\widehat{a}_2$ are the estimated magnitudes of the zeroth, first and second harmonic respectively. The symbols $\widehat{\Omega}_1$ and $\widehat{\Omega}_2$ are the phases corresponding to the first and second harmonics. The wind-field is parametrized by the finding values $\widehat{a}_0$, $\widehat{a}_1$, $\widehat{a}_2$, $\widehat{\Omega}_1$ and $\widehat{\Omega}_2$ that minimize the cost function. Specifically,

$$J = \left\{ \left[v_{r_n}\right] - \left[v_{r_{fit}}\right] \right\}^2 \quad (11)$$

Note that some authors use the number "$\frac{1}{2}$" in the cost function. This is typically done for ease of working with the derivatives of J. However, our implementation synthesizes a mesh of discrete values of a_0, a_1, a_2, Ω_1 and Ω_2, calculates J throughout this mesh and picks values that correspond to its minimum. Although computationally inefficient, this approach serves as a prognostic to visualize solution uniqueness. Finally, the mean baseline wind is retrieved as

$$\widehat{v}_{VAD-baseline} = \widehat{a}_1 sin(\widehat{\Omega}_1 + \phi_n) + \widehat{a}_2 sin(\widehat{\Omega}_2 + \phi_n) \quad (12)$$

Note that the zeroth harmonic is neglected from the VAD-like retrieval of baseline wind. This is because both known mechanisms that contribute to the zeroth harmonic (hydrometeor fall velocity and wind-field divergence) are nearly orthogonal to the baseline wind at low elevation angles. Fig. 2 compares simulated baseline wind retrievals from the various algorithms outlined in this section to theoretical expectations for a spatially constant wind-field that is radially oriented at scan angle $\phi = 0$ degrees. At $\phi = 90$ degrees, this same wind-field lies solely along the baseline. In addition to algorithm validation, simulation results show that spatially invariant wind-fields scanned by a radar produce radial and baseline velocities that are in quadrature.

III. Results

Fig. 3 shows observations of a convective rain event in Amherst, MA. Due to beam blockage issues, the maximum coverage was limited to about 270 degrees. Fig. 3a shows FFT-based spectrum width estimates on the convective rain event dataset. Note the region of large spectrum width at a range of about 10 Km, albeit its interpretation is ambiguous in the absence of dual-polarization radar observables. Fig. 3c-d shows the SNR at the left sub-array during the convective rain event. The SNR at the right sub-array (not shown) was similar.

Fig. 4 shows Doppler spectra and correlation function estimates at a range of 7.5 km in Fig. 3a. Based on performance on data and simulations, the following implementation of the FSA algorithm was most robust at X-band -

1) Subtract the long term mean of complex I/Q data from the left and right sub-arrays.
2) Divide 1.8 seconds worth of data into 6 segments of 300 ms duration.
3) Accumulate periodograms with 25% overlap to estimate the Power spectral density. Apply a phase compensation to the cross-spectrum based on Fourier shift theorem and correct for the time offset of 1 PRT due to alternating left/right sub-arrays.
4) Smooth the magnitudes of the accumulated periodogram using a 15 point moving-average filter. The smoothed periodogram of the Doppler spectrum at this stage is shown in Fig. 4a.
5) Sort the magnitudes of the DFT coefficients to estimate the cross-spectrum noise floor. When the cross-spectrum DFT coefficient magnitudes are less than 5 dB above the estimated noise floor or 10 dB below the peak of the smoothed cross-spectrum, set the corresponding values to 0. The filtered cross-spectrum at is shown in Fig. 4a.
6) From the filtered cross-spectrum $c_{12}(v)$, estimate first and second moments of the Doppler spectrum as

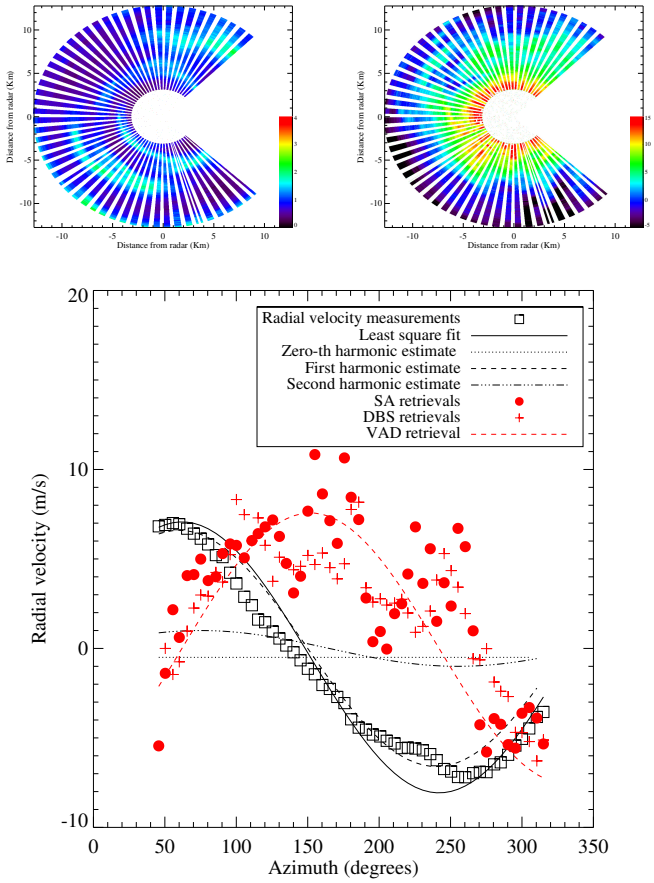

Fig. 3: Measurements from a convective storm in Amherst, MA using "stepped" mechanical scanning at 10 degrees elevation. Data is shown in wedges to reflect discrete and discontinuos azimuthal sampling every 5 degrees. Clockwise from top left. (a) FFT based spectrum width estimates. (b) Left spaced antenna sub-array SNR measurements. SNR measurements from the right spaced-antenna sub-array (not shown) is similar. (c) Qualitative comparison of spaced-antenna baseline wind estimates with Doppler beam swinging and velocity-azimuth display retrievals of baseline wind at a range of 7.5 Km.

$$\widehat{v}_r = \frac{\Sigma v |c_{12}(v)|}{\Sigma |c_{12}(v)|} \tag{13}$$

$$\widehat{\sigma}_w = \sqrt{\frac{\Sigma (v - \widehat{v}_r)^2 |c_{12}(v)|}{\Sigma |c_{12}(v)|}} \tag{14}$$

7) Where the DFT coeffient magnitudes exceed zero and within 2 estimated spectrum widths ($\widehat{\sigma_w}$) of the estimated Doppler velocity ($\widehat{v}_r$), a line is fit to the cross-spectral phase estimates. The linear fit and the points used for the fit is indicated in Fig. 4b.
8) Using estimates of spectrum width and slope of cross-spectral phase fit, retrieve baseline wind using equation (2).

Unlike the generalized FSA algorithm, the parametric G-SZL algorithm assumes a Gaussian form for the correlation functions [1]. The implementation of the G-SZL algorithm that yielded most robust results with data follows -

1) Subtract the long term mean of complex I/Q data from the left and right sub-arrays.
2) Estimate spectra using Bartlett method. The duration of the FFT is the duration of the dwell.
3) After applying spectral phase compensation, transform the data to the time-domain.
4) Estimate $\widehat{\tau}_c$ by fitting a Gaussian to 14 lags of the auto-correlation function (7 lags on either side of lag-zero). The cross-correlation coefficient at lag-zero is omitted due to its susceptibility to thermal noise induced "spiking".
5) Estimate $\widehat{\tau}_p$ by fitting a Gaussian to cross-correlation coefficients that exceed 0.1 or use 7 lags on either side of of lag-zero, whichever is more restrictive. To alleviate vulnerability to noise spikes, the lag-zero sample is omitted from the fit to the cross-correlation function. The fits along with the correlation coefficient estimates are indicated in Fig. 4c.
6) Retrieve baseline wind using equation (1).

Fig. 5 shows that both the G-SZL and FSA retrievals agree with DBS and VAD retrievals. For values exceeding the threshold of $\widehat{\sigma}_w \leq 2$ m/s and $SNR \geq 4$ dB, note the improved behaviour of the scatter points in Fig. 5b as compared to in Fig. 5a. This is consistent with the simulation predictions in [1]. The RMS errors of the FSA, G-SZL, DBS and VAD-like retrievals were 0.83 m/s (10 degree resolution), 0.56 m/s (10 degree resolution), 1.03 m/s (10 degree resolution) and 1.35 m/s (270 degree resolution) respectively. The mean spectrum width of all data points employed to produce Fig. 5 was 0.53 m/s. The reported RMS errors of the spaced-antenna retrievals is slightly worse than simulation predictions. In part, this is because inherent spatial variations in the probed wind-field cause an apparent increase in the quantity we refer to as RMS error.

IV. Summary

Herein, we presented an empirical evaluation of spaced-antenna retrievals using a weather radar. The executed experiment to compare SA retrievals to DBS and VAD-like variational retrievals utilized stepped motion of the beam such that there was no mechanical slewing during the dwell. On a dataset with smoothly varying wind-profiles, the SA retrievals were in quantitative agreement with the DBS and VAD retrievals for data points exceeding a quality control threshold. This 4-dB SNR and 2 m/s spectrum width threshold was determined using Monte-Carlo simulations.

The methodology employed in this work was reliant on a dataset with smooth wind-profiles and low wind-speeds. Based on results obtained on this dataset, the parametric time domain G-SZL algorithm outperformed the non-parametric spectral FSA algorithm. This is because as spectra slightly deviated from a Gaussian form, the correlation coefficients close to lag-zero remained largely unchanged. Time-domain ringing was far removed from lag-zero for the ubiquitous unimodal spectra in the dataset. On a stratiform rain case study, spaced-antenna weather radar retrievals were demonstrated

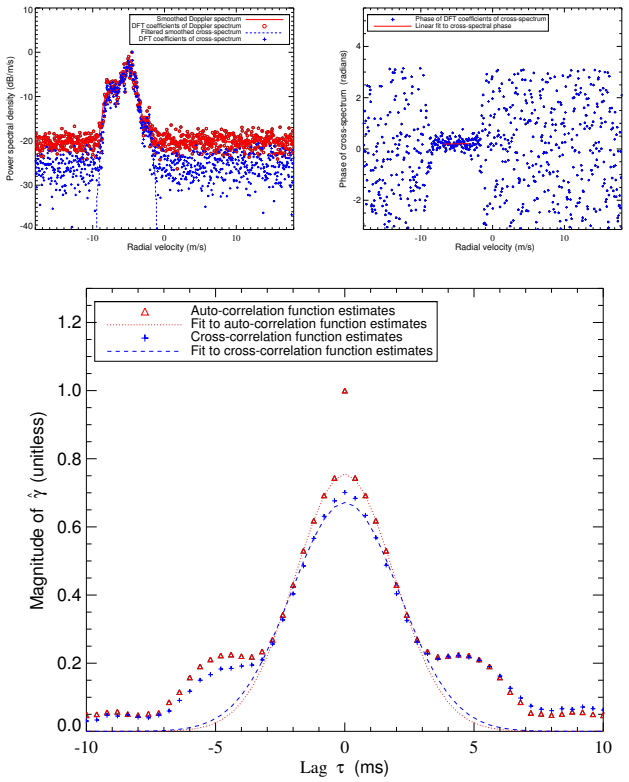

Fig. 4: Spectra and correlation function estimates at a range of 7.5 Km at an azimuth of approximately 215 degrees. Here, SNR = 5.28 dB. Clockwise from top left. (a) - Doppler and cross-spectral magnitudes. (b) - Cross-spectral phase. (c) - Auto- and cross-correlation functions. Correlation functions were estimated using the Bartlett method and the spectra were estimated using the Welch method. Baseline wind retrievals : $\widehat{v}_{G-SZL}$ = 2.79 m/s, $\widehat{v}_{FSA}$ = -1.73 m/s, $\widehat{v}_{DBS}$ = 2.65 m/s and $\widehat{v}_{VAD-baseline}$ = 2.73 m/s. Correlation function estimates : $\widehat{\tau}_p$ = 0.02 ms and $\widehat{\sigma}_w$ = 1.31 m/s. Spectral estimates : $\widehat{\tau}_p$ = -0.013 ms and $\widehat{\sigma}_w$ = 1.38 m/s.

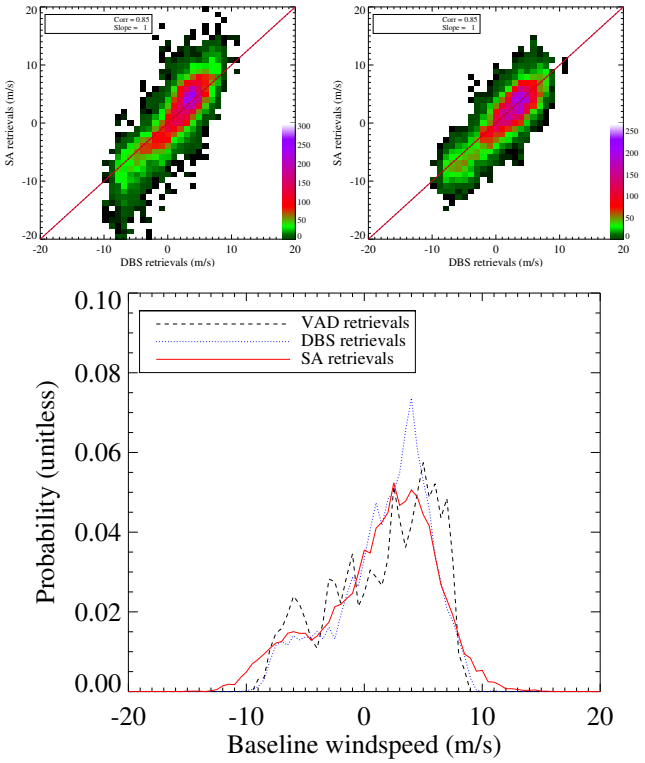

Fig. 5: Quantitative comparisons of spaced-antenna baseline wind measurements with other retrieval techniques. For data quality control, a threshold of $\widehat{\sigma}_w \leq 2\ m/s$ and SNR ≥ 4 dB were employed. Clockwise from top left. (a) - Comparison of FSA and DBS retrievals. (b) Comparison of G-SZL and DBS retrievals. (c) Probability density functions of baseline winds retrieved by the SA G-SZL, DBS and VAD algorithms.

at close range for relatively low to moderate wind-speeds. On datasets with higher wind-speeds (not investigated in this work), preliminary results from spaced-antenna retrievals sometimes yielded abnormally high wind-speeds at ranges exceeding 10 Km [2]. Notwithstanding, in these cases DBS and VAD-like variational retrievals also fail.

REFERENCES

[1] V. Venkatesh and S. Frasier, "Simulation of spaced-antenna wind retrieval performance for an x-band phased-array weather radar," *J. Atmos. Oceanic. Tech.*, vol. 30, pp. 1447–1459, 2013.

[2] G. Zhang and R. J. Doviak, "Spaced-antenna interferometry to measure crossbeam wind, shear and turbulence: Theory and formulation," *J. Atmos. Oceanic. Tech.*, vol. 24, pp. 791–805, 2007.

[3] V. Venkatesh, K. Orzel, and S. Frasier, "Spaced-antenna aperture synthesis using an x-band active phased array," *IEEE Geoscience and Remote Sensing Letters*, DOI:10.1109/LGRS.2020.2995360, 2020.

[4] T. A. Seliga and V. N. Bringi, "Potential use of radar differential reflectivity measurements at orthhogonal polarizations for measuring precipitation," *J. Appl. Meteor.*, vol. 15, pp. 69–75, 1976.

[5] T.-Y. Yu, M. B. Orescanin, C. D. Curtis, D. S. Zrnić, and D. E. Forsyth, "Beam multiplexing using the phased-array weather radar," *J. Atmos. Oceanic. Tech.*, vol. 24, pp. 616–626, 2006.

[6] N. Yossouf and D. J. Stensrud, "Impact of phased-array radar observations over a short assimilation period: Observing system simulation experiments using an ensemble kalman filter," *J. Atmos. Oceanic. Tech.*, vol. 138, pp. 517–538, 2010.

[7] B. Isom, R. Palmer, R. Kelley, J. Meier, D. Bodine, M. Yeary, B. Cheong, Y. Z. anf T. Yu, and M. I. Biggerstaff, "The atmospheric imaging radar : Simultaneous volumetric observations using a phased array weather radar," *J. Atmos. Oceanic. Tech.*, vol. 30, pp. 655–675, 2013.

[8] R. J. Doviak, R. J. Lataitis, and C. L. Holloway, "Cross correlations and cross spectra for spaced antenna wind profilers part I: Theoretical analysis," *Radio Sci.*, vol. 31, pp. 157–180, 1996.

[9] C. L. Holloway, R. J. Doviak, S. A. Cohn, R. J. Lataitis, and J. S. V. Baelen, "Cross correlations and cross spectra for spaced antenna wind profilers part II: Algorithms to estimate wind and turbulence," *Radio Sci.*, vol. 32, pp. RS3017, doi:10.1029/2003RS003 022, 1997.

[10] P. Wauldteufel and H. Corbin, "On the analysis on single doppler radar data," *Journal of Applied Meteorology*, vol. 18, pp. 532–542, 1979.

[11] R. Rinehart and E. Garvey, "Three dimensional storm motion detection by conventional weather radar," *Nature*, vol. 273, pp. 287–289, 1978.

[12] G. Zhang and R. J. Doviak, "Spaced-antenna interferometry to locate sub-volume inhomogeneties of reflectivity : An anology with monopulse radar," *J. Atmos. Oceanic. Tech.*, vol. 21, pp. 1921–1938, 2008.

[13] R. J. Doviak, G. Zhang, S. Cohn, and W. Brown, "Comparison of spaced-antenna baseline wind estimators: Theoretical and simulated results," *Radio Sci.*, vol. 39, p. doi:10.1029/2003RS002931, 2004.

[14] Y. Li, R. Doviak, and G. Zhang, "Crossbeam wind measurements using spaced-antenna and doppler beam swinging based on monopulse configurations with the national weather radar testbed," in *25th Conference on IIPS*. Phoenix, AZ: AMS, 2009, p. P2.1.